
This is an electronic reprint of the original article.
This reprint may differ from the original in pagination and typographic detail.

Sihvola, Ari; Wallen, Henrik; Yla-Oijala, Pasi; Parveen, Rashda

Backscattering enhancement, vanishing extinction, and morphological effects of active scatterers

Published in:
Journal of the Optical Society of America B: Optical Physics

DOI:
[10.1364/JOSAB.475441](https://doi.org/10.1364/JOSAB.475441)

Published: 01/01/2023

Document Version
Peer-reviewed accepted author manuscript, also known as Final accepted manuscript or Post-print

Please cite the original version:
Sihvola, A., Wallen, H., Yla-Oijala, P., & Parveen, R. (2023). Backscattering enhancement, vanishing extinction, and morphological effects of active scatterers. *Journal of the Optical Society of America B: Optical Physics*, 40(1), 194-205. <https://doi.org/10.1364/JOSAB.475441>

This material is protected by copyright and other intellectual property rights, and duplication or sale of all or part of any of the repository collections is not permitted, except that material may be duplicated by you for your research use or educational purposes in electronic or print form. You must obtain permission for any other use. Electronic or print copies may not be offered, whether for sale or otherwise to anyone who is not an authorised user.

Backscattering enhancement, vanishing extinction, and morphological effects of active scatterers

ARI SIHVOLA^{1,*}, HENRIK WALLÉN,¹ PASI YLÄ-OIJALA,¹ AND RASHDA PARVEEN²

¹ Department of Electronics and Nanoengineering, Aalto University, PO Box 15500, 00076 Aalto, Finland

² Department of Electronics, Quaid-i-Azam University, Islamabad, Pakistan

*ari.sihvola@aalto.fi

Abstract: Using analytical Lorenz–Mie scattering formalism and numerical methods, we analyze the response of active particles to electromagnetic waves. The particles are composed of homogeneous, non-magnetic, and dielectrically isotropic medium. Spherical scatterers and sharp and rounded cubes are treated. The absorption cross-section of active particles is negative, thus showing gain in their electromagnetic response. Since the scattering cross-section is always positive, their extinction can be either positive, negative, or zero. We construct a five-class categorization of active and passive dielectric particles. We point out the enhanced backscattering phenomenon that active scatterers display, and also discuss extinction paradox and optical theorem. Finally, using COMSOL Multiphysics and an in-house Method-of-Moments code, the effects of the non-sphericity of active scatterers on their electromagnetic response are illustrated.

© 2023 Optica Publishing Group

1. Introduction

Scattering by material particles is a classical problem in electromagnetics and optics. The effect of a scatterer on incoming waves is dependent, in addition to the size and shape of this object, also on its material constitution. In the present study, we focus on the electromagnetic response of particles that are characterized by active material properties. In other words, the medium displays gain. The problem to be treated consists of a scatterers which are non-magnetic, isotropic, and homogeneous, characterized by a uniform scalar (complex) permittivity. The objects to be analyzed are symmetric: spheres and cubes with varying rounding on their edges and corners. For the analysis of spherical scatterers, we apply the Mie theory, while for the non-spherical shapes, numerical approaches are used.

A solid foundation to analyze scattering by a sphere rests on the Lorenz–Mie scattering theory [1, 2]. Mie scattering is indeed a very proven theory to analyze, in a full-wave extension, the scattering, absorption, and extinction due to spherical particles exposed to electromagnetic and optical radiation. While there are, in the literature, several extensions of Mie theory to, for example, core–shell particles [3], layered structures [4], and spheres whose surface is defined by boundary conditions [5, 6], it seems that spheres with active response have attained much less attention. Some early theoretical studies on the electromagnetic response of active scatterers exist from 1970s [7–9], and also worth seeing is the later study on Kerker conditions [10]. The mechanisms to generate active responses (via external energy pumping and stimulated emission lasing) can be enhanced by strong resonance effects in nanoparticles with silver shell and gain-impregnated silica core [11], as well as quantum-dot active coated nanoparticles [12], where in the analysis classical homogenization is applied [13]. A core–shell structure can be "internally homogenized" using effective medium formulas applicable for dielectric mixtures [14, 15], and it turns out that also in the active regime, Maxwell Garnett homogenization turns out to be useful [16].

In the following, we define an active dielectric medium by the sign of the imaginary part of its permittivity. Following the time-harmonic notation $\exp(j\omega t)$, the complex relative permittivity reads $\varepsilon' - j\varepsilon''$ which means that a positive ε'' corresponds to lossy (dissipative) media, negative ε'' to gainy (active) media, and $\varepsilon'' = 0$ stands for lossless (and gainless) media [17, p. 91]. Gain materials are active while passive media $\varepsilon'' \geq 0$ comprise both the dissipative and lossless classes. The characterization of active and passive scatterers leads to an interesting classification of particles where we distinguish them based on the signs of their extinction cross section and the imaginary part of their permittivity. We show how the behavior of the multipolar electric and magnetic Mie coefficients is strongly dependent on the degree of activity, emphasize the strong backscattering enhancement for gainy particles, and revisit the fundamental concepts of extinction paradox and optical theorems. Numerical approaches are compared with the Mie series results and a good agreement is observed. These numerical approaches allow us to study how the shape of active scattering particles affects their electromagnetic and optical response.

2. Lorenz–Mie scattering by active spheres

The classical Lorenz–Mie analysis of the scattering process when an isotropic dielectric sphere in free space (background medium parameters are ε_0 and μ_0) is exposed to an electromagnetic wave leads to the scattering (sca), absorption (abs), and extinction (ext) cross sections of the scattering object. Here we follow the notation in the textbook by Bohren and Huffman [18]. Normalized by the geometric cross section of the sphere, the cross sections become dimensionless efficiencies which can be computed from the following series

$$Q_{\text{sca}} = \frac{2}{x^2} \sum_{n=1}^{\infty} (2n+1) (|a_n|^2 + |b_n|^2) \quad (1)$$

$$Q_{\text{ext}} = \frac{2}{x^2} \sum_{n=1}^{\infty} (2n+1) \text{Re} \{a_n + b_n\} \quad (2)$$

$$Q_{\text{abs}} = Q_{\text{ext}} - Q_{\text{sca}} \quad (3)$$

The electric and magnetic Mie coefficients a_n and b_n appearing in these expressions read, as functions of the relative permittivity ε and radius a of the sphere, as

$$a_n = \frac{\sqrt{\varepsilon} \psi_n(\sqrt{\varepsilon} x) \psi_n'(x) - \psi_n(x) \psi_n'(\sqrt{\varepsilon} x)}{\sqrt{\varepsilon} \psi_n(\sqrt{\varepsilon} x) \xi_n'(x) - \xi_n(x) \psi_n'(\sqrt{\varepsilon} x)} \quad (4)$$

$$b_n = \frac{\psi_n(\sqrt{\varepsilon} x) \psi_n'(x) - \sqrt{\varepsilon} \psi_n(x) \psi_n'(\sqrt{\varepsilon} x)}{\psi_n(\sqrt{\varepsilon} x) \xi_n'(x) - \sqrt{\varepsilon} \xi_n(x) \psi_n'(\sqrt{\varepsilon} x)} \quad (5)$$

where the dimensionless size parameter is $x = 2\pi a/\lambda$, with λ being the wavelength. Here, the Riccati–Bessel functions ψ_n, ξ_n are defined in terms of the ordinary spherical Bessel (j_n) and Hankel (h_n) functions:

$$\psi_n(\rho) = \rho j_n(\rho), \quad \xi_n(\rho) = \rho h_n^{(2)}(\rho), \quad (6)$$

The validity of the Mie expansions has been proven for dielectric, magnetic, lossless, and lossy spheres, as well as impedance-boundary scatterers for a myriad of applications during the past decades. However, due to the fact that not so many studies have been published for Mie scattering of active spheres, care has to be taken when the parametric space of the material character of the sphere is extended by changing the sign of the imaginary part of the permittivity. This is the focus of the present section where we look carefully on the convergence of the Mie series for active scattering spheres and compare with the known convergence behavior of the efficiency series for non-active scatterers. The comparison with numerical approaches is made to both to verify that our Mie code is correct and to assess the accuracy of the numerical approaches.

2.1. Wiscombe criterion and convergence of the Mie series

Since the scattering, absorption, and extinction efficiencies (1)–(3) are formally infinite series, they need to be truncated in the numerical evaluation. Electrically (optically) large spheres require more terms than small ones: the larger the size parameter x , the more terms are needed to maintain the accuracy. The widely-used rule in the existing literature is the so-called Wiscombe criterion [19]: the required minimum number of terms in the Mie series is

$$N = \begin{cases} \lceil x + 4x^{1/3} + 1 \rceil & x \leq 8 \\ \lceil x + 4.05x^{1/3} + 2 \rceil & 8 < x < 4200 \\ \lceil x + 4x^{1/3} + 2 \rceil & 4200 \leq x < 20,000 \end{cases} \quad (7)$$

where the symbol of ceiling $\lceil \cdot \cdot \cdot \rceil$ denotes the closest integer larger than the argument.

To illustrate the convergence of the Mie series and the validity of the Wiscombe criterion, Figure 1 shows the error of a truncated series for the extinction efficiency as function of the number of terms, for passive ($\varepsilon = 2 - j$) and active ($\varepsilon = 2 + j$) spheres with size parameter $x = 2$. The figure shows that the Wiscombe criterion is extremely conservative when computing the extinction efficiency: for $x = 2$, the Wiscombe criterion (7) requires 9 terms in the series, which, according to Figure 1, gives already 13 correct digits! Another interesting observation is that with a given number of terms N , the computed efficiency of the active sphere is more accurate than for the dissipative one, at least in this case.

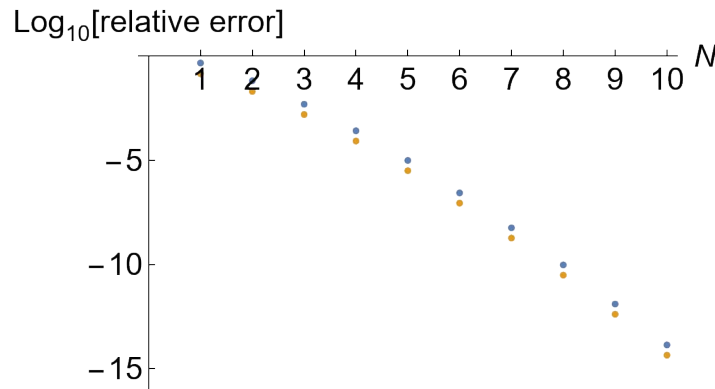


Figure 1. The relative error (the vertical axis shows the number of correct digits of the approximation) of the extinction efficiency Q_{ext} , as function of the number of terms N in the Mie expansion for $x = 2$. Blue dots: passive scatterer ($\varepsilon = 2 - j$); orange dots: active scatterer ($\varepsilon = 2 + j$).

One would expect that the convergence of the Mie series would be slower when the efficiency is very large, like at resonances, rather than at this arbitrary chosen case ($x = 2$, $\varepsilon = 2 \mp j$). Figure 2 shows the corresponding comparison at the first resonance of the active sphere ($x = 2.14$, $\varepsilon = 2 + j$) and the conjugate dissipative sphere ($x = 2.14$, $\varepsilon = 2 - j$). For this case, the efficiency of the active case converges much more rapidly than in Figure 1: for a given number of terms, the active sphere is three orders of magnitude more accurate than the dissipative (or lossless, $\varepsilon = 2$) case. For comparison, also shown is the fast convergence of the series for a lossless plasmonic (negative-permittivity) sphere.

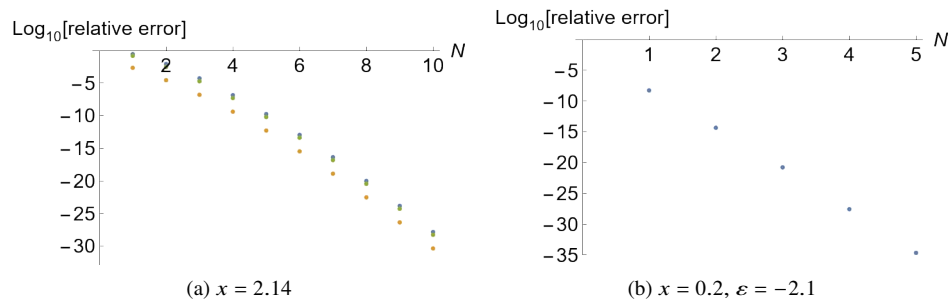


Figure 2. The relative error (the vertical axis shows the number of correct digits of the approximation) of the scattering efficiency Q_{sca} , as function of the number of terms N in the Mie expansion. (a) Blue dots: passive scatterer ($\epsilon = 2 - j$); orange dots: active scatterer ($\epsilon = 2 + j$), green dots: lossless scatterer ($\epsilon = 2$). (b) The same rapid convergence for a lossless plasmonic resonance (negative-permittivity sphere).

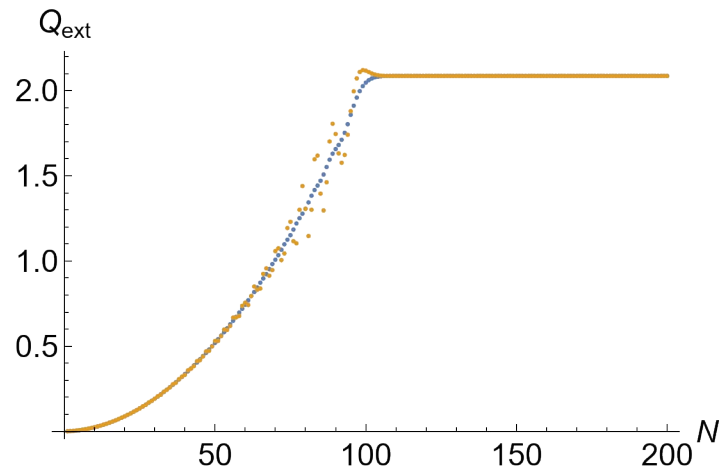


Figure 3. The convergence of the Mie series as the number of terms N for the extinction efficiency of passive (blue dots, $\epsilon = 2 - j$) and active (orange dots, $\epsilon = 2 + j$) large spheres (the size parameter $x = 100$).

Another look at the convergence is given in Figure 3 where the extinction efficiency estimate of large spheres ($x = 100$) is shown as the number of terms N in the Mie series increases. For this size, the Wiscombe criterion requires 121 terms, while in the figure, the curves stabilize already at around 100 terms. Extinction is very close but not equal for the passive ($\varepsilon = 2 - j$) and active ($\varepsilon = 2 + j$) cases: $Q_{\text{ext}} = 2.086$ and $Q_{\text{ext}} = 2.087$, respectively. Active and passive spheres seem to converge with similar speeds, but the convergence behavior of the passive one (blue dots) is more stable as N increases.

2.2. Extinction paradox

A strong theoretical result for the scattering problem is the so-called extinction paradox [20, 21], according to which in the high-frequency limit, the extinction cross section of the particle equals twice its geometrical cross section. In other words, the extinction efficiency Q_{ext} approaches the value 2 when x becomes large. This result has been validated for passive and perfectly conducting spheres, for which Q_{ext} converges to this value rather smoothly. The paradoxical nature of this result continues to excite discussion in the literature; see, for instance, the recent critical studies on the explanation of the extinction paradox [22–24].

Previous literature has not analyzed extinction paradox in the context of active spheres which motivates us to take a look into the behavior of the extinction of an optically large active sphere. Figure 4 displays the extinction efficiency of two cases of active spheres ($\varepsilon = 2 + j$ and $\varepsilon = 2 + j10$), as function of x . The figures show that the extinction curves of active objects differ radically from the corresponding passive ones: the extinction efficiency displays strong oscillations for moderate size parameters. Despite this, the result corroborates the extinction paradox also in the active case, as the curves stabilize close to the value 2 when x reaches values of around 40.

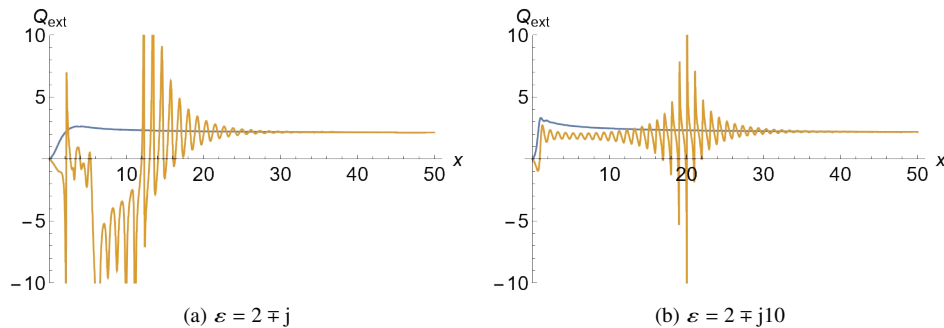


Figure 4. The extinction efficiency of active and passive spheres, for a wide variation of size parameter x . Blue curves are for passive and orange ones for active scatterers.

2.3. Comparison with numerical approaches

In this section, numerical solutions are compared with the Mie solutions for an active sphere. We use an in-house Method-of-Moments (MoM) code (based on [25, 26]) and commercial software COMSOL Multiphysics [27] which is based on the finite element method (FEM). Both methods are available for arbitrarily shaped particles.

In MoM, an electromagnetic scattering problem is reformulated as a surface integral equation (SIE) for equivalent electric \mathbf{J} and magnetic \mathbf{M} surface current densities. This yields surface mesh and surface unknowns, and the field behavior in a medium is described with a Green's function. Compared to the methods based on volume meshing, such as FEM, these properties could be particularly beneficial in active media where the fields inside the medium may have strong variations.

Let us take a look at the behavior of the Green's function in an active medium. This function is defined by

$$G(\mathbf{r}, \mathbf{r}') = \frac{e^{-jkR}}{4\pi R} = \frac{1}{4\pi R} (\cos kR - j \sin kR), \quad R = |\mathbf{r} - \mathbf{r}'| \quad (8)$$

with an active medium wave number ($\varepsilon'' < 0$)

$$k = \omega \sqrt{\varepsilon \varepsilon_0 \mu_0} = \omega \sqrt{\varepsilon' - j\varepsilon''} \sqrt{\varepsilon_0 \mu_0}. \quad (9)$$

The behavior of the Green's function in lossless ($\varepsilon = 3$), dissipative ($\varepsilon = 3 - 1.5j$) and active ($\varepsilon = 3 + 1.5j$) media is illustrated in Figure 5(a). In all three cases, the real part of the Green's function has $1/R$ type singularity as the field \mathbf{r} and source \mathbf{r}' points coincide, while the imaginary parts are regular as $R \rightarrow 0$. This indicates that similar singularity subtraction [28] or cancellation [29] techniques that are developed for the numerical evaluation of the Green's function in passive and lossless media would work also in the active case. The difference is that in active media the Green's function, both the real and imaginary parts, is a strongly oscillating function which amplitude increases as the distance between the field and source points increases. In passive dissipative medium the Green's function is decaying function as R increases.

In this work the classical Poggio–Miller–Chang–Harrington–Wu–Tsai (PMCHWT) [30] surface integral equation formulation with Rao–Wilton–Glisson (RWG) [31] basis and test functions is applied. Since this approach has not been previously applied for active objects, it is necessary to verify the correctness and accuracy of the solution. Figure 5(b) displays the results of this study versus the number of planar triangular for a passive (lossy) and an active sphere. In both cases the same analytical and numerical methods [25], which are previously developed for passive materials, and with the same number of integration points are used to evaluate the singular integrals involving the Green's function and its gradient. The results indicate that to obtain the same accuracy as in the passive case, higher mesh density is required in the active case, particularly as the size parameter x increases.

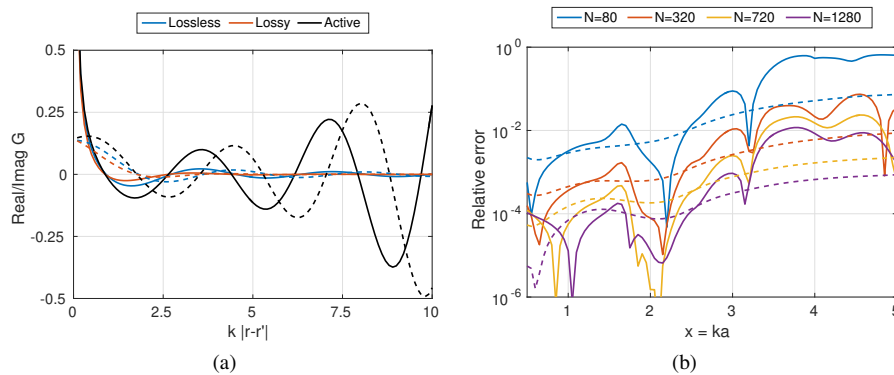


Figure 5. (a) Real (solid lines) and imaginary (dashed lines) parts of the Green's function in lossless, ($\varepsilon = 3$), dissipative ($\varepsilon = 3 - 1.5j$) and active ($\varepsilon = 3 + 1.5j$) media. (b) Relative error of the MoM solution for a passive sphere (dashed lines, $\varepsilon = 3 - 1.5j$) and active sphere (solid lines, $\varepsilon = 3 + 1.5j$) with increased number of planar triangular surface elements (N).

In COMSOL [27], the computational setup is similar to the verification example `rsc_sphere` that is included with the RF Module. To ensure good accuracy, we have maximum edge length $\lambda/10$ in the free tetrahedral meshes in the sphere and also in the air layer surrounding the sphere,

and an 8-layer swept mesh in the spherical perfectly matched layer (PML). Both the air layer and the PML are $\lambda_0/2$ thick. The scattering efficiency Q_{sca} is computed using a surface integral of the time average power outflow of the scattered field, while the absorption efficiency Q_{abs} is computed using a volume integral of the electromagnetic power loss density in the sphere.

A comparison of the efficiencies of an active sphere computed with Mie series, MoM code, and COMSOL software is shown in Figures 6 and 7. In the MoM solution the mesh is the same for all size parameters, while in COMSOL the thickness of the air layer and the PML relative to the sphere radius depend on the size parameter x and so also the mesh depends on x . Good accuracy is obtained with both numerical methods and they agree well with the Mie series results.

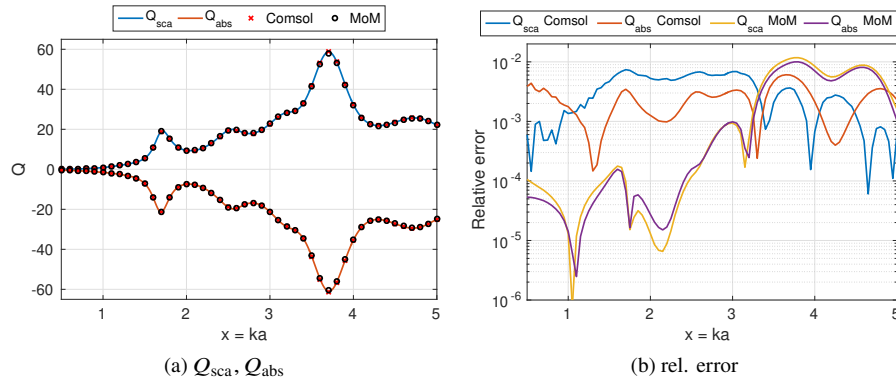


Figure 6. (a) Scattering and absorption efficiency with Mie series, COMSOL and in-house MoM code versus the size parameter $x = ka$. (b) Relative errors of COMSOL and MoM solutions for Q_{sca} and Q_{abs} . An active sphere with $\varepsilon = 3 + 1.5j$.

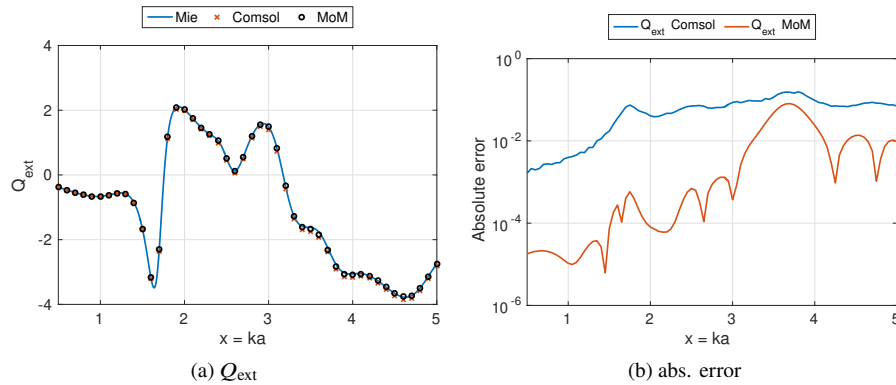


Figure 7. (a) Extinction efficiency with Mie series, COMSOL and in-house MoM code. (b) Absolute errors of the COMSOL and MoM solutions for Q_{ext} . An active sphere with $\varepsilon = 3 + 1.5j$.

3. Mie coefficients and backscattering enhancement

The behavior of the electric and magnetic Mie coefficients a_n and b_n determine the spectral characteristics of the scattering and extinction of the spheres with a given permittivity. It turns out that there is a drastic difference between the coefficients and consequently the global response of active dielectric spheres compared to passive and dissipative ones.

3.1. Properties of Mie coefficients

For lossless/gainless scatterers ($\varepsilon'' = 0$), the Mie coefficients satisfy

$$\operatorname{Re}\{c_n\} = |c_n|^2 \quad (10)$$

where c_n stands for both the electric (a_n) and magnetic (b_n) coefficients. From (10), it can be seen that the absolute value of the coefficients is always between 0 and +1. For dissipative scatterers, the maximum value is less than one, while for active scatterers, the coefficients do not have an upper limit. A comparison of Mie coefficients (Figure 8) for the three types of scatterers illustrates these properties.

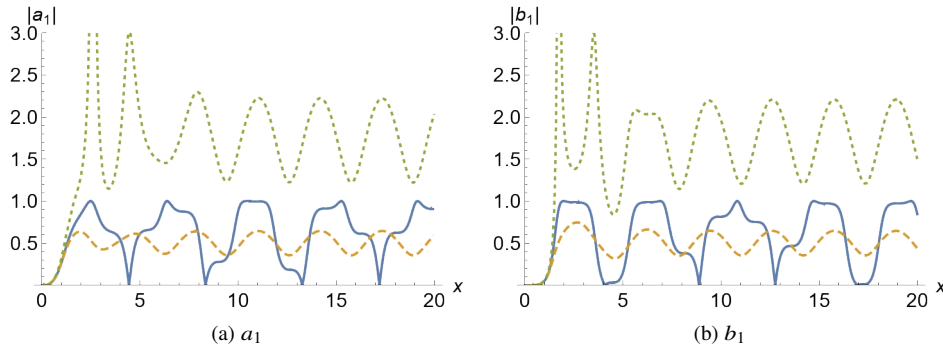


Figure 8. Comparison of Mie coefficients as function of the size parameter x for a lossless ($\varepsilon = 3$, solid blue), dissipative ($\varepsilon = 3 - j$, dashed orange), and active ($\varepsilon = 3 + j$, dotted green) non-magnetic sphere.

An interesting result for the Mie coefficients (valid for all x, n , and $\varepsilon = \varepsilon' - j\varepsilon''$) is the following:

$$2c_n(\varepsilon)c_n^*(\varepsilon^*) = c_n(\varepsilon) + c_n^*(\varepsilon^*) \quad (11)$$

where the conjugate of a complex number is denoted by $\varepsilon^* = (\varepsilon' - j\varepsilon'')^* = \varepsilon' + j\varepsilon''$. For lossless scatterers ($\varepsilon'' = 0$), Equation (11) returns the result (10). This formula (11) provides a straightforward way to compute the Mie coefficients of an active sphere from the corresponding passive ones.

3.2. Multipolar contributions to the efficiencies

As an example of how the different multipoles contribute to the scattering of a sphere, consider an active sphere with relative permittivity $\varepsilon = 2 + j$ as function of its size. Figure 9 displays how the various electric and magnetic multipoles account for the total scattering efficiency Q_{sca} . It is noteworthy that the main, rather sharp, resonance at around $x = 2.1$ is due to the magnetic dipole while the other resonances from higher-order modes remain softer and take place for optically larger spheres. This is indeed dramatically different from the behavior of passive scatterers for which the magnetic dipole resonance cannot be distinguished as a separate peak in the scattering cross section plot for scatterers with relative permittivity as low as $\varepsilon' = 2$.

Another perspective how the electric and magnetic multipoles contribute to scattering is shown in Figure 10. There the contribution of electric and magnetic multipoles into the scattering and absorption efficiencies of an active sphere with $\varepsilon = 3 + j1.5$ is illustrated separately. Note the fact that, concerning the magnetic multipoles, only the magnetic dipole b_1 has a notable effect; all other resonances in scattering and absorption efficiencies arise from the electric multipoles a_n .

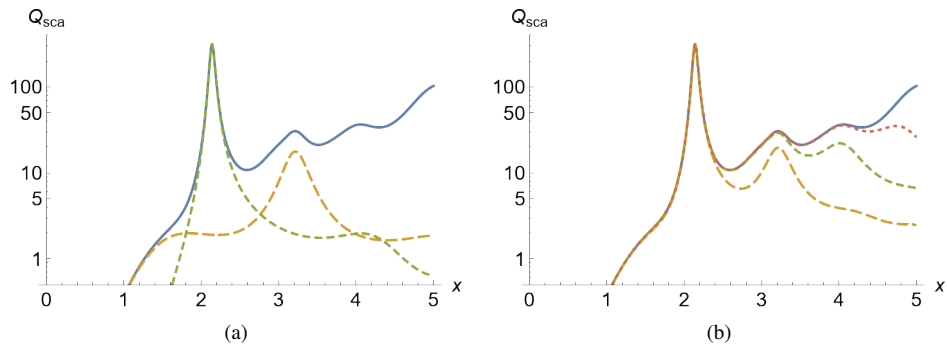


Figure 9. (a) The contributions of the electric dipole scattering corresponding to the coefficient a_1 (long-dashed orange) and the magnetic dipole from coefficient b_1 (short-dashed green) into the total scattering efficiency Q_{sca} (solid blue), as function of the size parameter x . (b) The contributions of the orders of multipoles: both dipoles ($n = 1$; long-dashed orange), dipoles and quadrupoles ($n = 1, 2$; short-dashed green), and dipoles, quadrupoles, and hexapoles ($n = 1, 2, 3$; dotted red). The results are for an active sphere with $2 + j$.

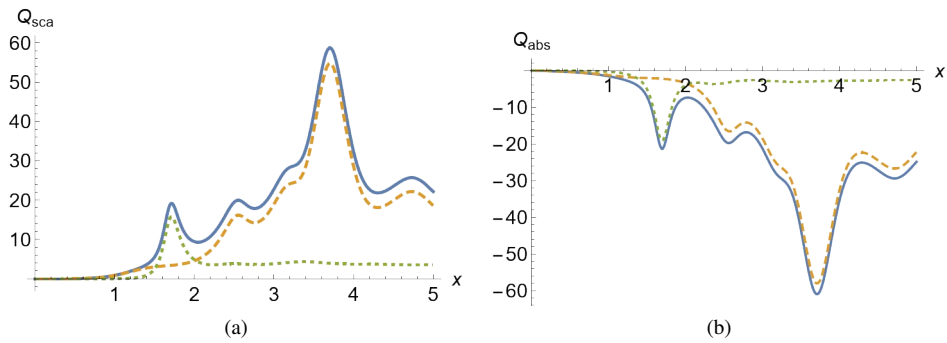


Figure 10. (a) The contribution of electric multipoles (orange dashed) and magnetic multipoles (green dotted) to the scattering efficiency (blue solid) as function of the size parameter x . (b) The same for the absorption efficiency. The results are for an active sphere with $\epsilon = 3 + j1.5$.

3.3. Backscattering enhancement

In our previous short study, we have emphasized the particular character in the scattering behavior of active dielectric objects: the enhanced backscattering [32]. This section illustrates the characteristics of the backscattering behavior of active spheres, emphasizes the notable difference in scattering in comparison with passive spheres, and connects the phenomenon with the dipolar Mie coefficients and the so-called second Kerker condition.

From the Mie coefficients, the backscattering and forward scattering cross sections and efficiencies (Q_b and Q_f) can be computed:

$$Q_b = \frac{1}{x^2} \left| \sum_{n=1}^{\infty} (2n+1) (-1)^n (a_n - b_n) \right|^2 \quad (12)$$

$$Q_f = \frac{1}{x^2} \left| \sum_{n=1}^{\infty} (2n+1) (a_n + b_n) \right|^2 \quad (13)$$

As the imaginary part of the permittivity of a sphere changes sign, its forward-to-backward scattering cross section Q_f/Q_b changes drastically. This is illustrated in Figure 11 for spheres with varying size (the real part of the relative permittivity is kept constant $\epsilon' = 3$). There it can be seen that while for passive spheres $\epsilon'' > 0$ this ratio is of the order of unity and decreases when the size parameter becomes larger, for negative ϵ'' values, it has a very dynamic behavior and can reach very large values.

Another way of illustrating the backscattering enhancement is the asymmetry parameter g which weighs the scattering over all the spatial directions [18, p. 72]:

$$g = \langle \cos \theta \rangle = \frac{Q_{\text{sca}} \langle \cos \theta \rangle}{Q_{\text{sca}}} \quad (14)$$

where

$$Q_{\text{sca}} \langle \cos \theta \rangle = \frac{4}{x^2} \sum_{n=1}^{\infty} \frac{n(n+2)}{n+1} \text{Re} \{a_n a_{n+1}^* + b_n b_{n+1}^*\} + \frac{4}{x^2} \sum_{n=1}^{\infty} \frac{2n+1}{n(n+1)} \text{Re} \{a_n b_n^*\} \quad (15)$$

Positive values of g indicate that the object scatters mostly into the forward hemisphere while negative values mean that the backward scattering is dominant. This is also shown in Figure 11.

While the enhanced backscattering is responsible for much of the large Q_b/Q_f values (and negative g values) in Figure 11, this ratio can also be locally large due to very low forward scattering cross section. For example, for a sphere with $x = 1.65$ and $\epsilon = 3 + j2$, the back-to-forward ratio is around 17.2 and $g \approx -0.423$. This can be connected to the *second Kerker condition* for which the electric and magnetic dipole Mie coefficients a_1 and b_1 are opposite complex numbers, leading to a vanishing dipole contribution in Equation (13) for the forward scattering efficiency [33]. Indeed, for these values, the coefficients are

$$a_1 \approx 0.739 + j1.16 \quad \text{and} \quad b_1 \approx -0.789 - j1.10 \quad (16)$$

4. Zero-extinction objects

4.1. Classification of passive and active scatterers

Depending on the sign of the imaginary part of the permittivity of an object, it can be dissipative $\epsilon'' > 0$, lossless (and gainless) $\epsilon'' = 0$, or active $\epsilon'' < 0$, keeping in mind the time-harmonic notation $\exp(j\omega t)$ and the electrical engineering convention $\epsilon = \epsilon' - j\epsilon''$. Passive media are characterized by $\epsilon'' \geq 0$, including both lossless and dissipative cases. The scattering efficiency

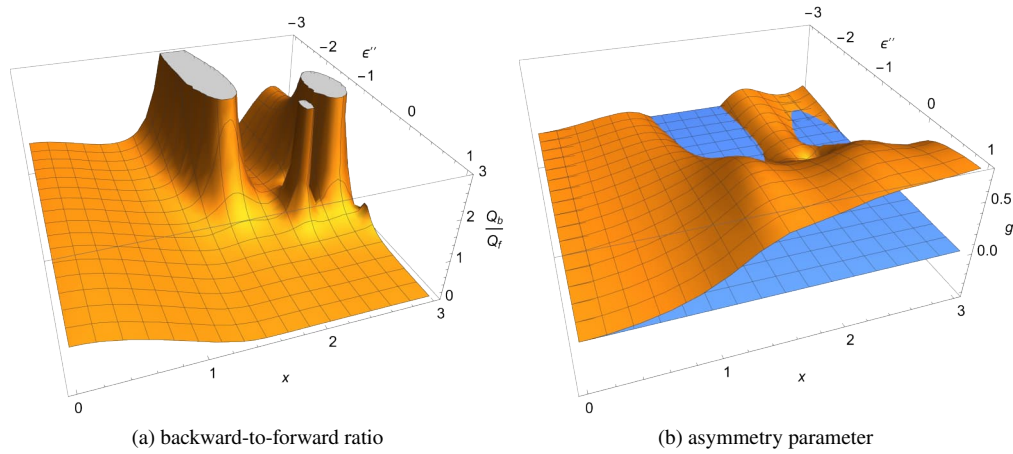


Figure 11. Illustration of the balance between backscattering and forward scattering of active $\epsilon'' < 0$ and dissipative $\epsilon'' > 0$ spheres, with real part of the relative permittivity being $\epsilon' = 3$, as function of the size parameter x and the imaginary part ϵ'' . The blue plane shows the level $g = 0$.

(1) is always positive regardless of the sign of ϵ'' , but the absorption efficiency (3), which has the same sign as ϵ'' , can be positive, zero, or negative, as has been pointed out previously [34, 35]. This means that for active scatterers, the sign of the extinction efficiency (2) can also vary. We can hence define three classes of active objects: positive extinction, zero extinction, and negative extinction objects, leading to the classification in Table 1.

	ϵ''		Q_{sca}	Q_{abs}	Q_{ext}
DPE	> 0	dissipative (positive extinction)	> 0	> 0	> 0
LPE	$= 0$	lossless (positive extinction)	> 0	$= 0$	> 0
APE	< 0	active (positive extinction)	> 0	< 0	> 0
AZE	< 0	active (zero extinction)	> 0	$= -Q_{sca}$	$= 0$
ANE	< 0	active (negative extinction)	> 0	< 0	< 0

Table 1. Five classes of scatterers (two passive and three active), determined by the signs of the absorption and extinction efficiencies.

4.2. Zero-extinction scatterers

The three efficiencies, as Table 1 shows, can combine with different signs when the parameters of the object change. While extinction is always positive for passive scatterers, the active side is very dynamic as the sign of extinction varies. In Figures 12–14 the character of the extinction efficiency is illustrated within the parametric space of the scatterers (the size and complex permittivity). The gray and white domains signify the sign of extinction. While the dissipative side of the figures ($\epsilon'' < 0$) is always gray (denoting positive extinction), on the active side the landscape is more varied. The three scatterer types (APE, AZE, and ANE) populate themselves into a complex variety of domains and surfaces within the three-dimensional $(x, \epsilon', \epsilon'')$ parameter

space of the sphere. Zero-extinction (AZE) objects are located on the boundaries between the white and gray regions in the figures.

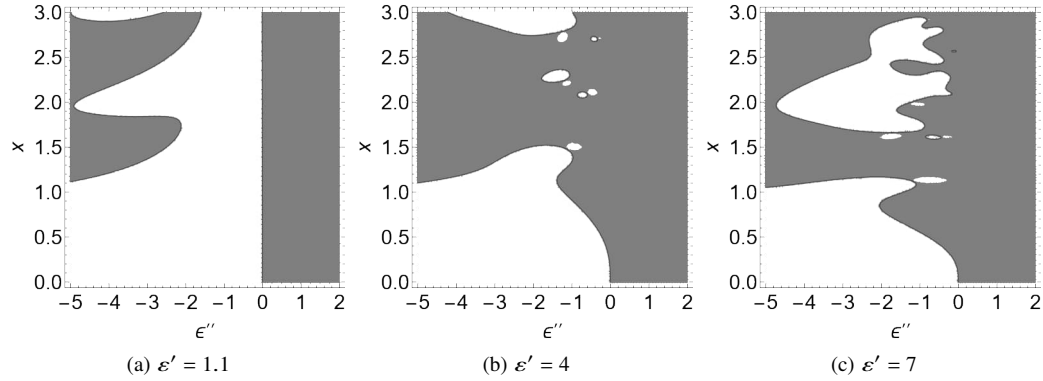


Figure 12. The sign of the extinction efficiency of dielectric spherical scatterers depicted as gray (APE and DPE, $Q_{\text{ext}} > 0$) and white (ANE, $Q_{\text{ext}} < 0$) in the plane with axes of the imaginary part of the relative permittivity ϵ'' and the size parameter of the sphere x . Note the rich structure of extinction variation on the active side ($\epsilon'' < 0$).

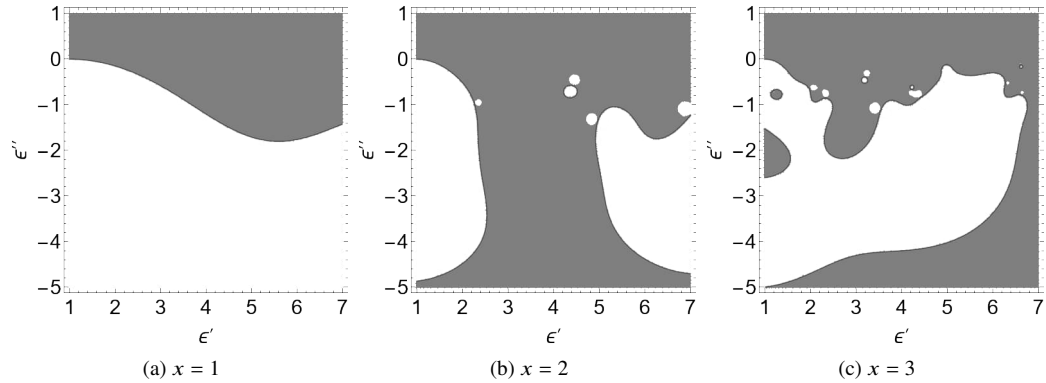


Figure 13. The sign of the extinction efficiency, as in Figure 12, but as function of the real (ϵ') and imaginary (ϵ'') parts of the permittivity.

4.3. Optical theorem

The so-called *optical theorem* in the scattering theory has a long history which starts already from 150 years ago, with the studies by John William Strutt (who later rose in peerage as Lord Rayleigh) [36, 37]. This fundamental theorem connects the extinction efficiency of an object to its forward scattering characteristics.

Using the notation in Bohren and Huffman [18, p. 112], the extinction cross section of a sphere is connected to the scattered field into the forward direction ($S(0^\circ)$) as

$$C_{\text{ext}} = \frac{4\pi}{k^2} \text{Re}\{S(0^\circ)\} \tag{17}$$

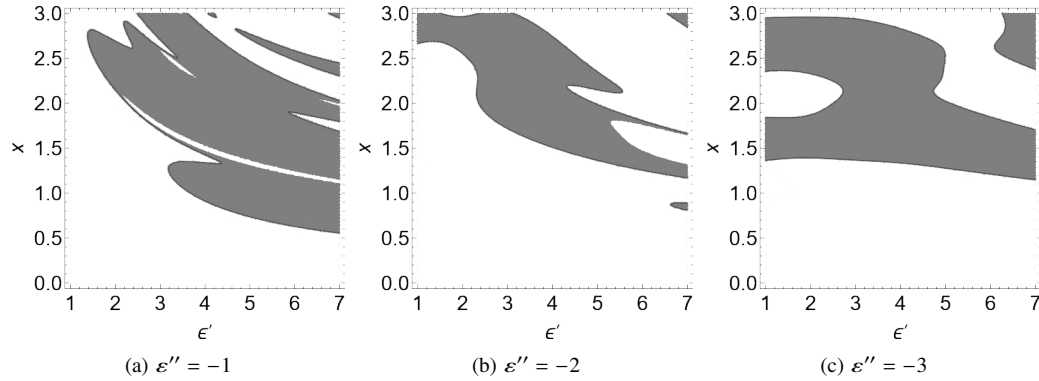


Figure 14. The sign of the extinction efficiency, as in Figure 12, but as function of the size parameter x and the real part of the permittivity ϵ' .

where

$$S(0^\circ) = \frac{1}{2} \sum_n (2n+1)(a_n + b_n) \quad (18)$$

This gives us a form of the optical theorem:

$$Q_{\text{ext}} = \frac{4}{x^2} \text{Re}\{S(0^\circ)\} \quad (19)$$

For passive scatterers, the connection has been established in the past literature. Taking arbitrary parameters, like, for example $\epsilon = 2.3 - j1.2$ and $x = 3.4$, we have

$$Q_{\text{ext}} = 2.76096 \quad \text{and} \quad \frac{4}{x^2} S(0^\circ) = 2.76096 + j0.14832 \quad (20)$$

The optical theorem seems particularly relevant in the special case of AZE scatterers for which the extinction cross section vanishes. However, this does not mean that the forward scattering should vanish; only the real part of $S(0^\circ)$ according to (19). Let us confirm this result numerically by taking an AZE sphere $\epsilon = 2 + j$ with $x = 2.69156$. In this case we find that

$$Q_{\text{ext}} \approx 0 \quad \text{and} \quad \frac{4}{x^2} S(0^\circ) \approx j3.40627 \quad (21)$$

in agreement with the optical theorem.

5. Morphological effects on scattering response by active particles

So far the scattering response of spherical objects has been investigated. In this section we study qualitative effects of the shape of an active particle on the response of scattering and extinction characteristics. We proceed with another symmetric object, a cube, in which case we consider four different wave incidences and polarizations: face-on, edge-on (E), edge-on (H), and vertex-on. These are defined in Figure 15 by the vector directions: electric field (\mathbf{E}), magnetic field (\mathbf{H}), and the incident wave propagation direction (\mathbf{k}).

Figures 16 and 17 show the scattering, absorption and extinction efficiency for a cube having the same volume as a sphere with size parameter $x = ka$. The efficiency is normalized using the geometrical cross section of the cube, and given for the four incident fields mentioned above. The results computed with both COMSOL and MoM are shown. The scattering response

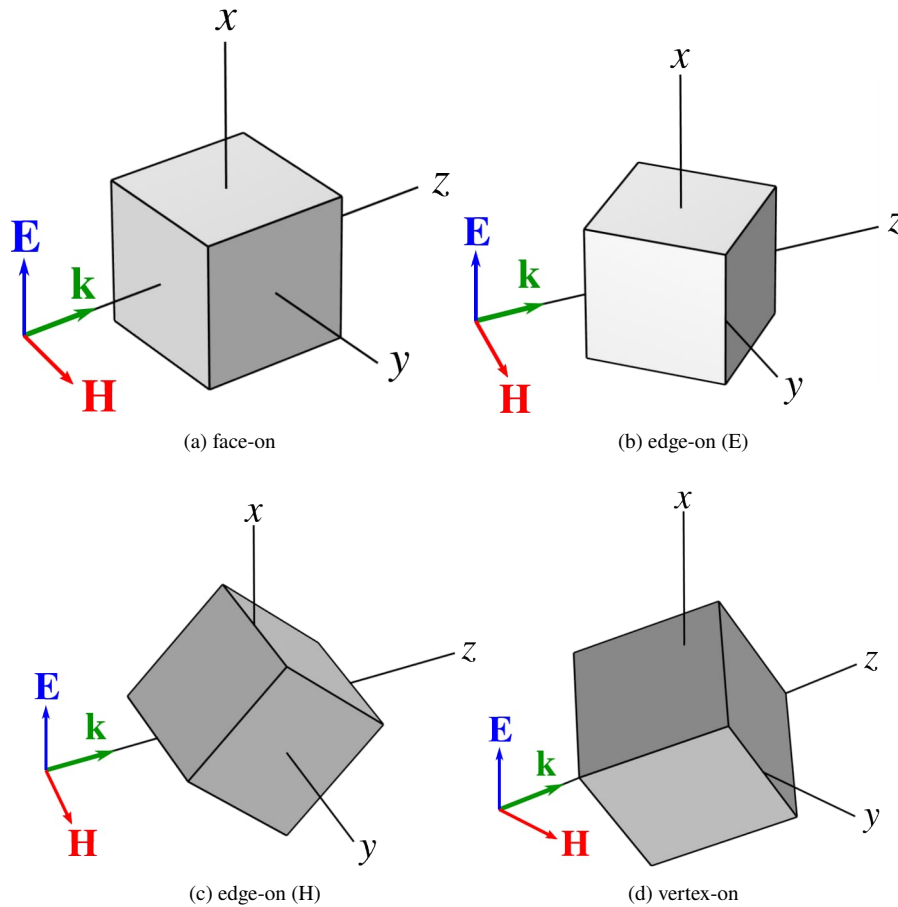


Figure 15. The four different excitations with electric field (\mathbf{E}), magnetic field (\mathbf{H}), and the z -directed incident wave propagation direction (\mathbf{k}).

(efficiency) and the geometrical cross section depend on the incident field propagation direction and polarization, except in the face-on and vertex-on cases where the solutions are independent on the incident field polarization.

To study the effect of the shape of an active particle on the response of scattering and extinction characteristics, the transformation of a sharp cube into a sphere is considered next. The geometries (rounded cubes) used in this study are illustrated in Figure 18. Figure 19 shows the scattering and absorption efficiency with face-on polarization. At the first two resonances (maxima of the efficiency) close to $x = 1.7$ and $x = 2.6$, the effect of this transformation on the efficiency is relative smooth, while for other resonances at larger x values the situation is more complicated.

To illustrate the field behavior at the resonances, we take a look at the near-field solutions of active particles. Figures 20 and 21 show the electric field at the xz -plane for an active sphere and cube with $\varepsilon = 3 + 1.5j$. In both cases the field is plotted for four different size parameters corresponding to the maxima of the scattering efficiency in Figure 6 and in Figure 16, respectively. The incident field is a $+z$ -propagating plane wave with an x -polarized electric field.

Clearly, the first two resonances of the sphere and cube are due to similar field solutions. This may also be concluded from Figure 19 where the first two maxima of Q_{sca} for a sphere and cube are relative close to each other, at $x = 1.71$ and $x = 2.55$ (sphere) and at $x = 1.75$ and $x = 2.60$ (cube). Also at the third resonances ($x = 3.7$ for a sphere and $x = 3.5$ for a cube) we

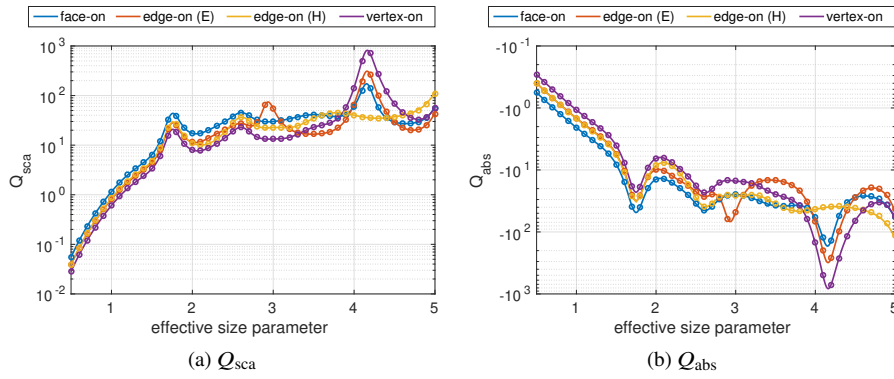


Figure 16. Scattering (a) and absorption (b) efficiency with COMSOL (solid lines) and MoM (circles) in logarithmic scale for a cube with $E = 3 + 1.5j$ and with four different incident waves. The cube has the same volume as a sphere with size parameter $x = ka$.

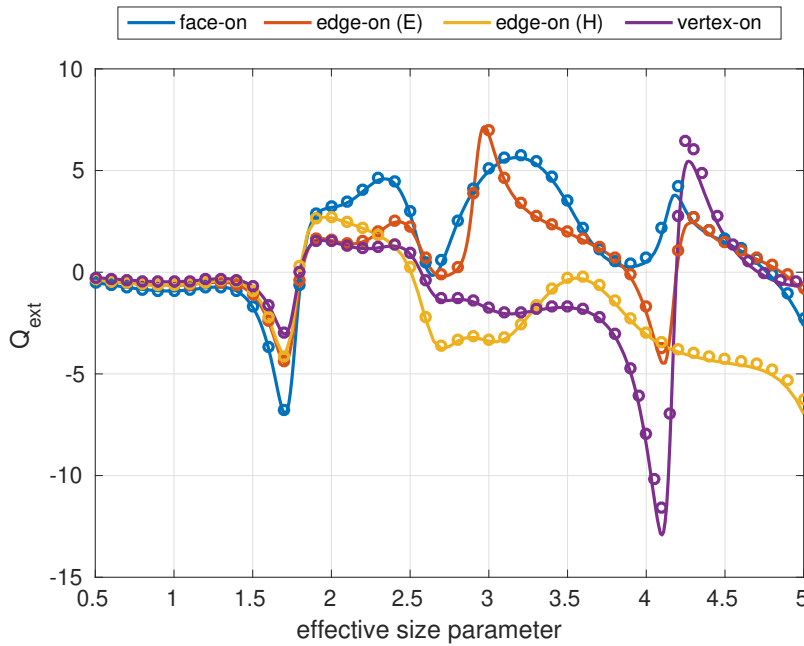


Figure 17. Extinction efficiency with COMSOL (solid lines) and MoM (circles) for a cube with $\epsilon = 3 + 1.5j$ and with four different incident waves, as in Figure 16.

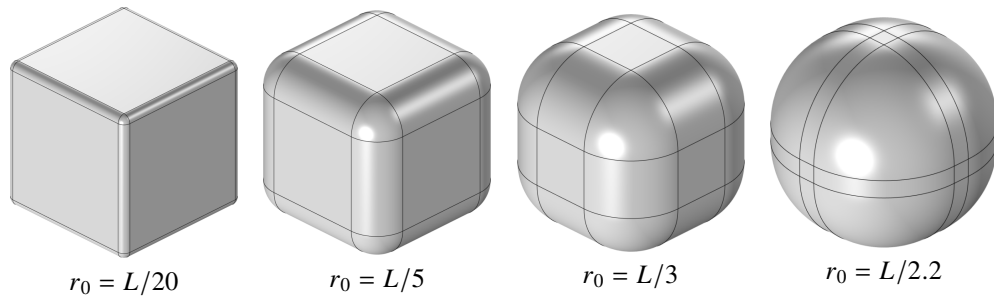


Figure 18. Geometry of a rounded cube with side length L and different fillet radius r_0 . From left to right a smooth transition from a slightly rounded cube to almost a sphere.

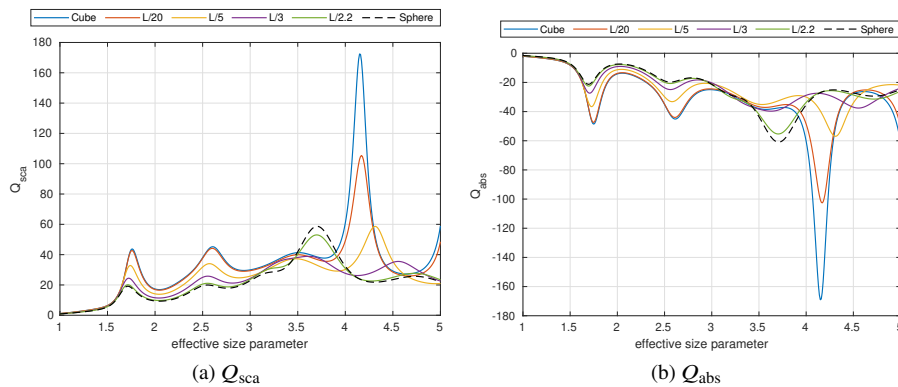


Figure 19. Scattering (a) and absorption (b) efficiency for an active cube with $\varepsilon = 3 + j1.5$ transforming into a sphere and face-on polarization. The geometry of the intermediate steps are shown in Figure 18. For a sphere the results are computed with Mie series, in other cases COMSOL solutions are shown. All scatterers have the same volume and the efficiency is normalized using the geometrical cross section of each object.

may recognize some similarities in the field solutions. The situation with the fourth resonances, however, is more complicated and a clear correspondence between the field solutions is not recognized. We note that for a cube with $x = 4.15$ (Figure 21(d)) the fields are strongly localized to the vertices and exactly the same field solution may not exist for a sphere.

6. Conclusion

The scattering response of material particles to electromagnetic and optical wave excitation depends strongly on their geometry and medium constitution. This paper focused on the absorption, scattering, and extinction of non-magnetic objects whose permittivity is isotropic but active (gainy), in other words, the imaginary part of the permittivity has the opposite sign than particles that are dissipative. Since the electromagnetic response of the scatterer needs to be described by absorption and extinction, in addition to the scattering, we arrived at an interesting classification of the objects (DPE, LPE, APE, AZE, ANE), depending on the sign (positive, zero, or negative) of the extinction cross section.

Lorenz–Mie theory was applied in most of the computations. Among the interesting results was the characteristic property of electromagnetically active particles that they tend to direct scattering into the backward half plane and their strong back-to-front scattering ratio. Nevertheless, there are strong theoretical identities, like the extinction paradox and optical theorem, that remain valid

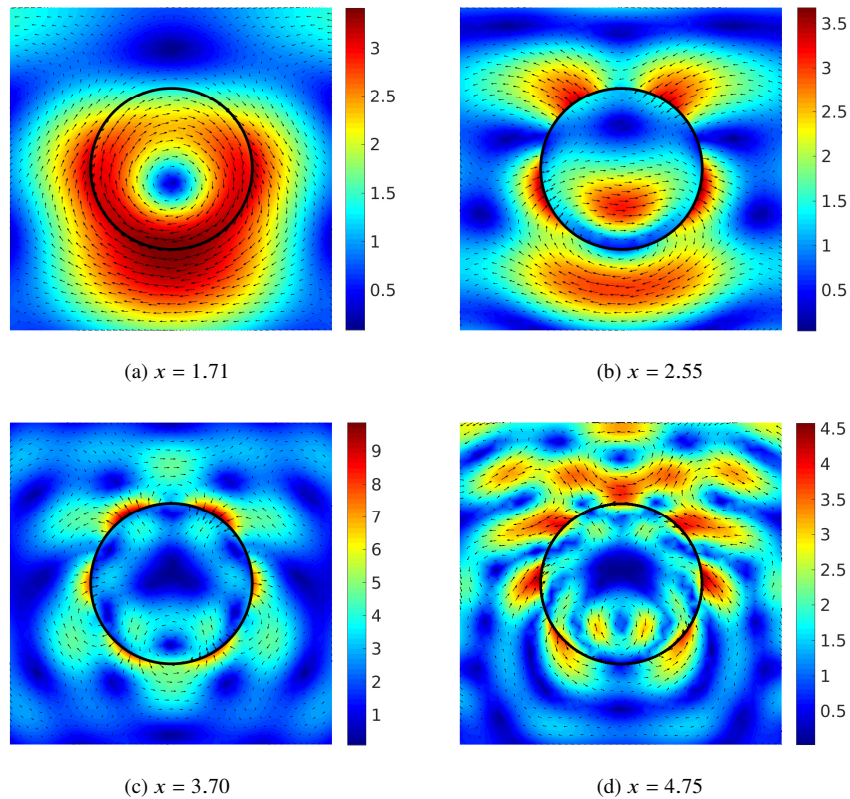


Figure 20. Electric field (computed with Mie series) at the xz -plane for an active sphere with $\varepsilon = 3 + 1.5j$ and with different size parameters. The incident field is propagating along the $+z$ axis and incident electric field is x polarized. Color indicates magnitude (color scale varies in the figures) and arrows show the direction of the field. In the figures, x -axis is horizontal and z -axis vertical.

even if the scatterer is active. These were discussed. Finally, using numerical approaches (Method of Moments and finite-element-based codes), the focus was on scatterer shapes differing from sphere (sharp and rounded cubes). The scattering spectrum of the particles and the position of the resonances evolves along with the change of the geometry from a sphere towards a cube, leading to a possibility for sensing the particle shape using the data of its electromagnetic scattering response.

Disclosures. The authors declare no conflicts of interest.

Data Availability Statement. Data underlying the results presented in this paper are not publicly available at this time but may be obtained from the authors upon reasonable request.

References

1. L. Lorenz, "Lysbevægelse i og uden for en af plane Lysbølger belyst Kugle," Kongelige Danske Videnskabernes Selskabs Skrifter **6**, 2–62 (1890).
2. G. Mie, "Beiträge zur Optik trüber Medien, speziell kolloidaler Metallösungen," Ann. der Physik **25**, 377–445 (1908).
3. A. L. Aden and M. Kerker, "Scattering of electromagnetic waves from two concentric spheres," J. Appl. Phys. **22**, 1242–1246 (1951).
4. R. L. Hightower and C. B. Richardson, "Resonant Mie scattering from a layered sphere," Appl. Opt. **27**, 4850–4855 (1988).

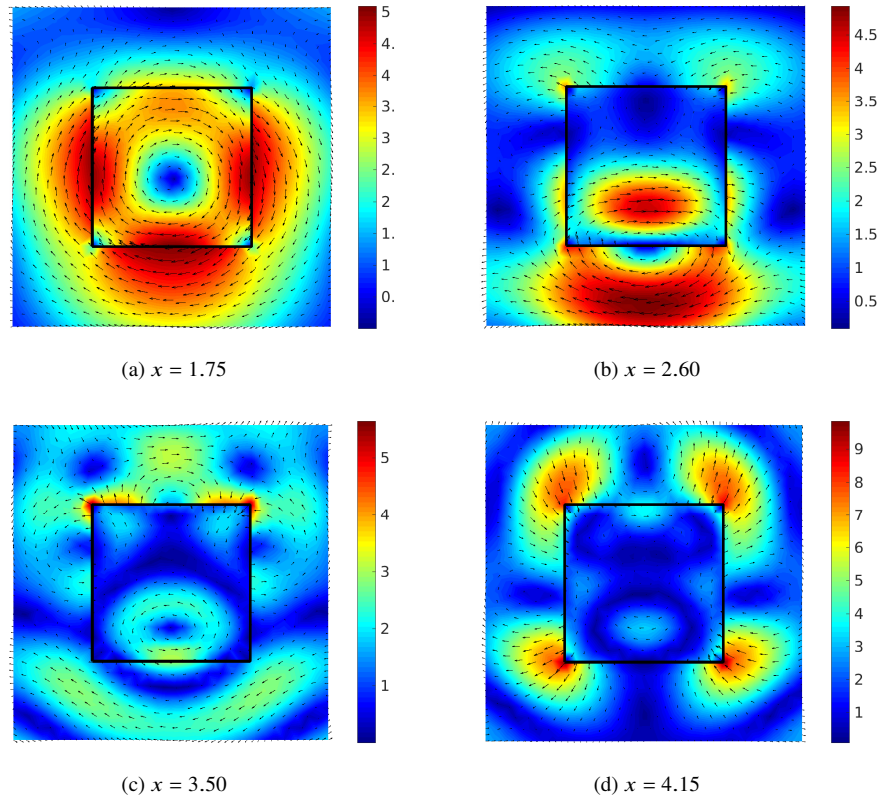


Figure 21. Electric field (computed with MoM) at the xz -plane for an active cube with $\varepsilon = 3 + 1.5j$ and with different size parameters. The incident field is propagating along the $+z$ axis and incident electric field is x polarized. In the figures, x -axis is horizontal and z -axis vertical.

5. H. Wallén, I. V. Lindell, and A. Sihvola, "Mixed-impedance boundary conditions," *IEEE Trans. on Antennas Propag.* **59**, 1580–1586 (2011).
6. A. Sihvola, B. Kong, P. Ylä-Ojala, D. C. Tzarouchis, and H. Wallén, "Scattering, extinction, and albedo of impedance-boundary objects," *URSI Radio Sci. Lett.* **1**, doi = 10.46620/19-0009 (2019).
7. N. G. Alexopoulos and N. K. Uzunoglu, "Electromagnetic scattering from active objects: invisible scatterers," *Appl. Opt.* **17**, 235–239 (1978).
8. M. Kerker, "Electromagnetic scattering from active objects," *Appl. Opt.* **17**, 3337–3339 (1978).
9. M. Kerker, "Resonances in electromagnetic scattering by objects with negative absorption," *Appl. Opt.* **18**, 1180–1189 (1979).
10. J. Olmos-Trigo, C. Sanz-Fernández, D. R. Abujetas, J. Lasa-Alonso, N. de Sousa, A. García-Etxarri, J. A. Sánchez-Gil, G. Molina-Terriza, and J. J. Sáenz, "Kerker conditions upon lossless, absorption, and optical gain regimes," *Phys. Rev. Lett.* **125**, 073205 (2020).
11. J. A. Gordon and R. W. Ziolkowski, "The design and simulated performance of a coated nano-particle laser," *Opt. Express* **15**, 2622–2653–1509 (1980).
12. J. Geng, R. W. Ziolkowski, R. Jin, and X. Liang, "Numerical study of the near-field and far-field properties of active open cylindrical coated nanoparticle antennas," *IEEE Photonics J.* **3**, 1093–1110 (2011).
13. P. Holmström, L. Thylén, and A. Bratkovsky, "Dielectric function of quantum dots in the strong confinement regime," *J. Appl. Phys.* **107**, 064307 (2010).
14. U. Chettiar and N. Engheta, "Internal homogenization: Effective permittivity of a coated sphere," *Opt. Express* **20**, 22976–86 (2012).
15. A. Sihvola, H. Kettunen, and H. Wallén, "Mixtures and composite particles: Correspondence of effective description," *2013 Int. Symp. on Electromagn. Theory* pp. 908–911 (2013).
16. S. D. Campbell and R. W. Ziolkowski, "The performance of active coated nanoparticles based on quantum-dot gain

- media.” *Adv. OptoElectronics* **2012** (2012).
17. I. V. Lindell, *Methods for Electromagnetic Field Analysis* (Oxford University Press and IEEE Press, Oxford, 1992, 1995).
 18. C. F. Bohren and D. R. Huffman, *Absorption and scattering of light by small particles* (Wiley, New York, 1983).
 19. W. J. Wiscombe, “Improved Mie scattering algorithms,” *Appl. Opt.* **19**, 1505–1509 (1980).
 20. L. Brillouin, “The scattering cross section of spheres for electromagnetic waves,” *J. Appl. Phys.* **20**, 1110–1125 (1949).
 21. G. Kristensson, *Scattering of Electromagnetic Waves by Obstacles* (SciTech Publishing, IET, Edison, New Jersey, 2016).
 22. M. J. Berg, C. M. Sorensen, and A. Chakrabarti, “Extinction and the optical theorem. Part I. Single particles,” *J. Opt. Soc. Am. A* **25**, 1504–1513 (2008).
 23. M. J. Berg, C. M. Sorensen, and A. Chakrabarti, “Extinction and the optical theorem. Part II. Multiple particles,” *J. Opt. Soc. Am. A* **25**, 1514–1520 (2008).
 24. M. Berg, C. Sorensen, and A. Chakrabarti, “A new explanation of the extinction paradox,” *J. Quant. Spectrosc. Radiat. Transf.* **112**, 1170–1181 (2011).
 25. P. Ylä-Oijala and M. Taskinen, “Calculation of CFIE impedance matrix elements with RWG and nxRWG functions,” *IEEE Trans. Antennas Propag.* **51**, 1837–1846 (2003).
 26. P. Ylä-Oijala, M. Taskinen, and J. Sarvas, “Surface integral equation method for general composite metallic and dielectric structures with junctions,” *Prog. In Electromagn. Res.* **52**, 81–108 (2005).
 27. COMSOL, “COMSOL Multiphysics® simulation software,” <https://www.comsol.com/comsol-multiphysics>. Version 6.0 released in Dec 2021.
 28. D. Wilton, S. Rao, A. Glisson, D. Schaubert, O. Al-Bundak, and C. Butler, “Potential integrals for uniform and linear source distributions on polygonal and polyhedral domains,” *IEEE Trans. on Antennas Propag.* **32**, 276–281 (1984).
 29. M. Khayat and D. Wilton, “Numerical evaluation of singular and near-singular potential integrals,” *IEEE Trans. on Antennas Propag.* **53**, 3180–3190 (2005).
 30. A. J. Poggio and E. K. Miller, “Integral equation solutions of three-dimensional scattering problems,” in *Computer Techniques for Electromagnetics*, R. Mittra, ed. (Pergamon, Oxford, UK, 1973), chap. 4, pp. 159–264.
 31. S. Rao, D. Wilton, and A. Glisson, “Electromagnetic scattering by surfaces of arbitrary shape,” *IEEE Trans. on Antennas Propag.* **30**, 409–418 (1982).
 32. A. Sihvola, R. Parveen, H. Wallén, and P. Ylä-Oijala, “Enhanced backscattering for dielectrically active scatterers,” *URSI Radio Sci. Lett.* **3**, DOI: 10.46620/21–0020 (2021).
 33. M. Kerker, D.-S. Wang, and C. L. Giles, “Electromagnetic scattering by magnetic spheres,” *J. Opt. Soc. Am.* **73**, 765–767 (1983).
 34. M. Kerker, D.-S. Wang, H. Chew, and D. D. Cooke, “Does Lorenz-Mie scattering theory for active particles lead to a paradox?” *Appl. Opt.* **19**, 1231–1232 (1980).
 35. M. Kerker, “Lorenz–Mie scattering by spheres: Some newly recognized phenomena,” *Aerosol Sci. Technol.* **1**, 275–291 (1982).
 36. J. W. Strutt, “XV. On the light from the sky, its polarization and colour,” *The London, Edinburgh, Dublin Philos. Mag. J. Sci.* **41**, 107–120 (1871).
 37. R. G. Newton, “Optical theorem and beyond,” *Am. J. Phys.* **44**, 639–642 (1976).